Journal of Earthquake and Tsunami
Vol. 6, No. 1 (2012) 1250004 (24 pages)

DOI: 10.1142/S1793431112500042

World Scientific
www.worldscientific.com

SEISMIC LATERAL FORCE DISTRIBUTION FOR DUCTILITY-BASED DESIGN OF STEEL PLATE SHEAR WALLS

SWAPNIL B. KHARMALE and SIDDHARTHA GHOSH*

Department of Civil Engineering
Indian Institute of Technology Bombay
Mumbai 400076, India
**sghosh@civil.iitb.ac.in*

Received 2 February 2011
Accepted 16 June 2011

The thin unstiffened steel plate shear wall (SPSW) system has now emerged as a promising lateral load resisting system. Considering performance-based design requirements, a ductility-based design was recently proposed for SPSW systems. It was felt that a detailed and closer look into the aspect of seismic lateral force distribution was necessary in this method. An investigation toward finding a suitable lateral force distribution for ductility-based design of SPSW is presented in this paper. The investigation is based on trial designs for a variety of scenarios where five common lateral force distributions are considered. The effectiveness of an assumed trial distribution is measured primarily on the basis of how closely the design achieves the target ductility ratio, which is measured in terms of the roof displacement. All trial distributions are found to be almost equally effective. Therefore, the use of any commonly adopted lateral force distribution is recommended for plastic design of SPSW systems.

Keywords: Steel plate shear wall; displacement-based design; ductility-based design; lateral force distribution; performance-based seismic design.

1. Introduction

The most commonly adopted seismic design practice for buildings is based on the equivalent static approach in which the dynamic inertial forces due to seismic vibration are represented by equivalent static forces. The distribution of equivalent lateral static forces at each floor level (where the seismic masses are lumped) of a multi-degree of freedom (MDOF) system is based on the first (fundamental) mode of vibration of the cantilevered structure. Commonly, the fundamental mode shape is more simplistically presented as a function of the floor height (h_i):

$$\phi_{i1} = \frac{h_i^k}{H}, \tag{1}$$

*Corresponding author.

where ϕ_{i1} is the ith floor amplitude of the first mode shape, h_i is the height of the ith floor from the base, and H is the building height. The index k indicates the nature of the fundamental mode, limited between a linear ($k = 1$) and a parabolic ($k = 2$) variation with the height. For a very rigid system, the fundamental mode shape approximates a linear variation, and for a very flexible system, the fundamental mode approximates a parabolic variation. The generic expression for the lateral load distribution factor is:

$$C_{vi} = \frac{w_i h_i^k}{\sum_{j=1}^{n} w_j h_j^k}, \tag{2}$$

where n is the total number of floors and w_i is the seismic weight of the ith floor. Different design standards recommend different values for k; for example, 1 in the erstwhile Uniform Building Code (UBC) [ICBO, 1997], 2 in the Indian Standard IS 1893 (Part 1) [BIS, 2002], and in the International Building Code (IBC) [ICC, 2006] and ASCE 7 [ASCE, 2005] — 1 for T_1 (fundamental period) less than 0.5 s, 2 for T_1 greater than 2.5 s, and a linear interpolation for T_1 between 0.5 and 2.5 s.

The assumption of a dominant fundamental mode and the corresponding linear to parabolic mode shape is valid only for low-rise and regular buildings. The second limitation is that the height-wise lateral force distribution as per Eq. (2) is valid only for linear elastic systems. Although most existing design codes suggest a linear elastic force-based design approach, this design method also implicitly assumes (through the use of a response reduction factor, R) that the structure will be inelastic when subjected to the design earthquake. In order to overcome this limitation, the performance-based seismic design (PBSD) philosophy [SEAOC, 1995; FEMA, 2006] proposes various design approaches which consider the inelastic behavior of the structure explicitly. For example, in the displacement-based approach, the design criterion is based on a target inelastic displacement, inelastic interstory drift or ductility demand. It is uncertain if such a design concept, which focuses primarily on the structural responses at plastic limit states, can still use the linear elastic fundamental mode-shape-based lateral force distribution. Adaptive pushover analyses [Kalkan and Kunnath, 2007], which focus on the lateral load distribution and deformed shape during the inelastic response of a structure, suggest that new lateral force distribution formulas need to be developed to handle inelastic response. Although adaptive modal pushover approaches [Gupta and Kunnath, 2000; Kalkan and Kunnath, 2006; Shakeri *et al.*, 2010] represent the changes in structural behavior (as the structure transits from an elastic to elastoplastic regime) better, most seismic design standards to date do not recommend the use of adaptive load distributions. Instead, an invariant force vector is usually recommended.

A performance-based design approach that was developed over the past decade focusing entirely on the inelastic behavior of structures is the performance-based plastic design (PBPD) method [Goel and Chao, 2009]. Research works at the University of Michigan [Lee and Goel, 2001; Chao and Goel, 2005] on the inelastic displacement-based design of steel structures (moment resisting frames (MRFs),

eccentrically braced frames, etc.) came up with specific recommendations for lateral force distribution considering the inelastic state of structure. Their proposed format was based on a shear proportioning factor β_i for the ith story:

$$C_{vi}^{s} = (\beta_i - \beta_{i+1}) \left(\frac{w_n h_n}{\sum_{j=1}^{n} w_j h_j} \right)^{\alpha T_1^{-0.2}}, \tag{3}$$

where β_i is defined as:

$$\beta_i = \frac{V_i}{V_n} = \left(\frac{\sum_{j=1}^{n} w_j h_j}{w_n h_n} \right)^{\alpha T_1^{-0.2}}, \tag{4}$$

β_{n+1} is equal to 0 in Eq. (3). The value of the parameter α was originally proposed as 0.5 and then was later modified to 0.75 [Chao *et al.*, 2007]. The proposed distribution was found to work well for the plastic design of a variety of steel framing systems (MRF, EBF, STMF, and CBF) and reinforced concrete frames as well.

Ghosh *et al.* [2009] developed a similar ductility-based design method for steel plate shear wall (SPSW) structures, where they used the PBPD force distribution recommended by Lee and Goel [2001] for steel MRFs. Ghosh *et al.* [2009] also tested two other lateral load distributions [Chao and Goel, 2005; ICC, 2006] by applying these to a few sample design cases, and the proposed method remained effective in achieving the target ductility for these two distributions as well. Although the proposed method gave satisfactory results using this distribution, these tests were based on a very small sample size and various other commonly adopted distributions were not tested. Ghosh *et al.* [2009] recommended that a suitable distribution needs to be found out specifically for the SPSW systems. The requirement for a suitable lateral force distribution for the displacement-based design of SPSW systems, in general, is the primary motivation for the work presented here. This paper focuses on finding a suitable lateral load distribution for the design of SPSWs, considering their inelastic behavior.

2. Methodology for Checking the Suitability of a Trial Distribution

A trial-based approach is selected to arrive at the seismic lateral force distribution most suitable for inelastic displacement-based design of SPSWs. A brief overview of this design procedure proposed by Ghosh *et al.* [2009] is presented here. Their method involves the seismic design of a SPSW system considering a certain ductility ratio and a specific yield mechanism as the target. The target ductility ratio (μ_t) is based on the roof displacement (D):

$$\mu_t = D_m / D_y, \tag{5}$$

where D_m is the maximum roof displacement subjected to an earthquake and D_y is the yield roof displacement. D_y for an SPSW structure is obtained from the

conventional nonlinear static pushover analysis (NSPA) using the lateral load distribution recommended in the IBC [ICC, 2006]. The base shear (V_b) versus roof displacement (D) pushover plot is bilinearized using an elastic-perfectly plastic force-deformation behavior, so that the areas under the pushover curve and its bilinear approximation are equal (Fig. 1). μ_t for a design should be selected based on the target performance limit state subjected to the selected ground hazard. The design method also sets a specific yield mechanism as target and thus controls the distribution of inelasticity (and in turn, interstory drift) over a building frame. All the designs considered in this work are based on a target yield mechanism (Fig. 2),

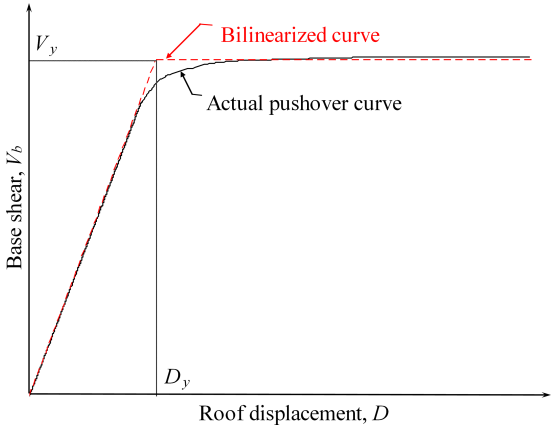

Fig. 1. Obtaining the yield base shear (V_y) and yield displacement (D_y) from the bilinearized pushover plot.

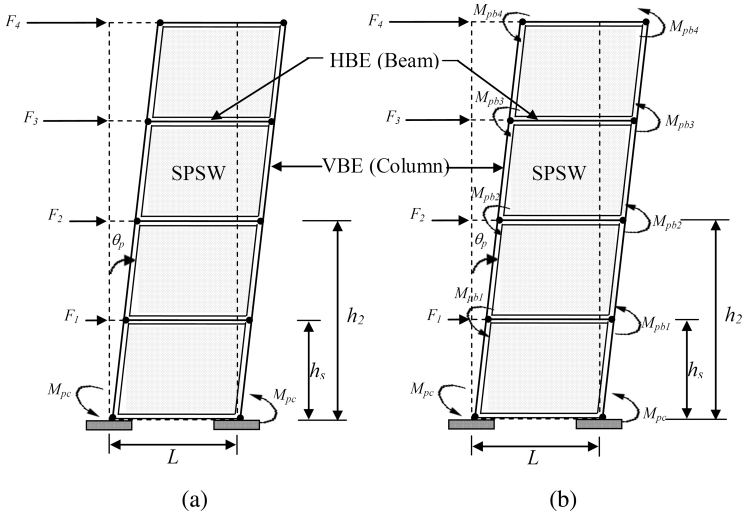

Fig. 2. Selected yield mechanism for the SPSW systems with (a) pin-connected beams and (b) rigid HBE–VBE connections.

where

- all the steel panels become fully plastic,
- plastic hinges form at the bases of the two vertical boundary elements (VBEs), and
- (for the SPSW with rigid HBE–VBE connections) plastic hinges form at both ends of all the beams.

Designs are based on specific ground acceleration records, or its pseudo-velocity (S_v) spectrum. However, a design can also be based on a design response spectrum. The goodness of a design is judged by how close the achieved ductility ratio (μ_a) is to the target (μ_t). μ_a is measured by calculating D_m from a nonlinear response–history analysis (NLRHA) subjected to the ground acceleration for which the structure is designed. Design flowcharts are provided in Figs. 3 and 4, and further details are available in Ghosh *et al.* [2009] and Kharmale and Ghosh [2010].

The step-by-step displacement-based design procedure for SPSW with pinned HBE–VBE connections [Ghosh *et al.*, 2009] is summarized here:

(1) For a selected μ_t, assume the fundamental time period (T_1) of the structure. A preliminary estimate can be made using the expression for T_{eq} given by Chopra and Goel [2001].
(2) Assume a suitable yield drift (θ_y). In general, it ranges from 0.75% to 1.0%. Calculate the plastic drift (θ_p) based on μ_t and the assumed θ_y.
(3) From the elastic pseudo-velocity spectra of the selected earthquake, obtain the pseudo-spectral velocity (S_v) corresponding to T_1 and assumed damping ratio (ζ). Calculate the elastic force coefficient (C_e) in terms of the pseudo-spectral acceleration (S_a):

$$C_e = \frac{S_v T_1}{2\pi g} = \frac{S_a}{g}. \tag{6}$$

(4) Calculate the energy modification factor (γ) [Lee and Goel, 2001]:

$$\gamma = \frac{2\mu_t - 1}{R_\mu^2}, \tag{7}$$

where R_μ is the ductility reduction factor and can be calculated using Newmark's method [Newmark and Hall, 1982] for the estimated T_1 and selected μ_t.
(5) Assume a suitable lateral force distribution ($\mathbf{f}$) and calculate the yield base shear (V_b):

$$\frac{V_b}{W} = \frac{-\alpha + \sqrt{\alpha^2 + 4\gamma C_e^2}}{2}, \quad \text{where } \alpha = \left(\sum_{i=1}^{n} C_{vi} h_i\right) \frac{8\theta_p \pi^2}{T_1^2 g}. \tag{8}$$

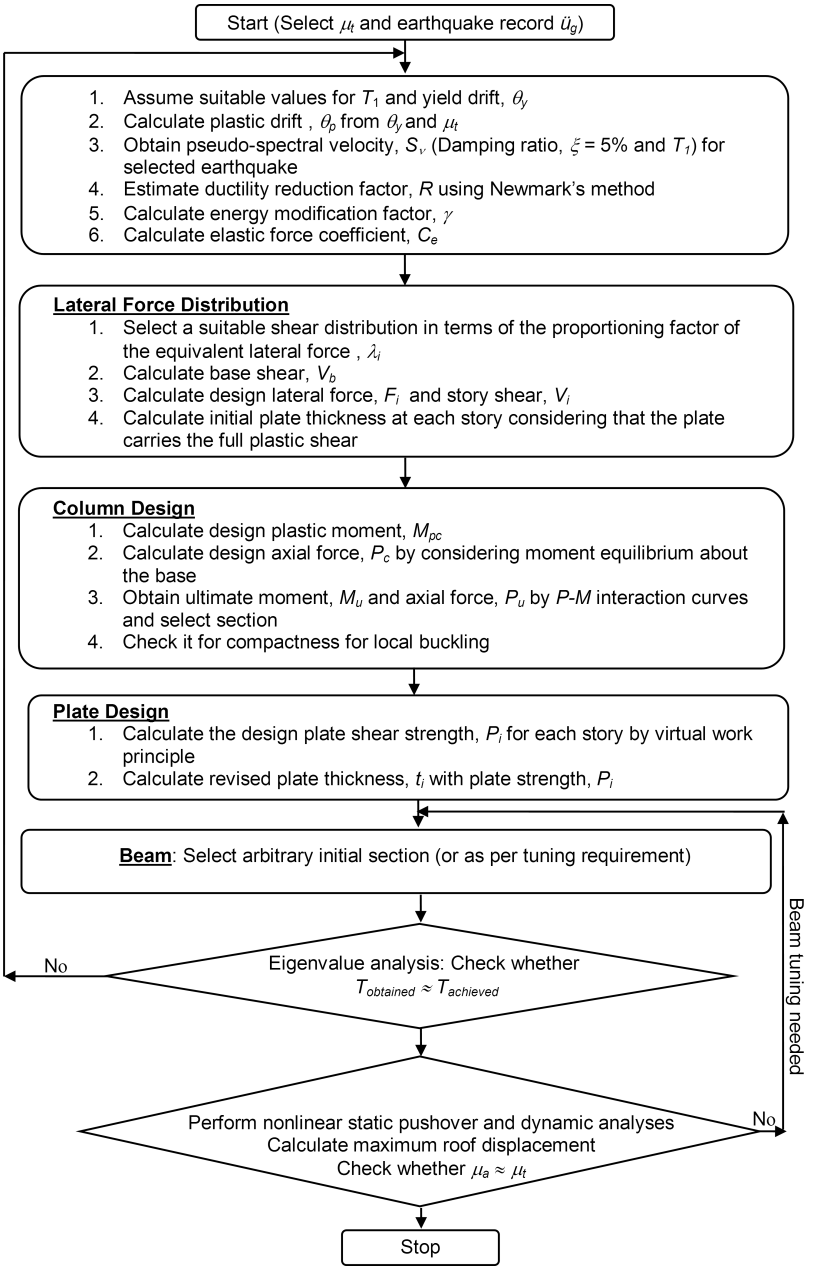

Fig. 3. Step-wise displacement-based design procedure for SPSW with pin-connected beams.

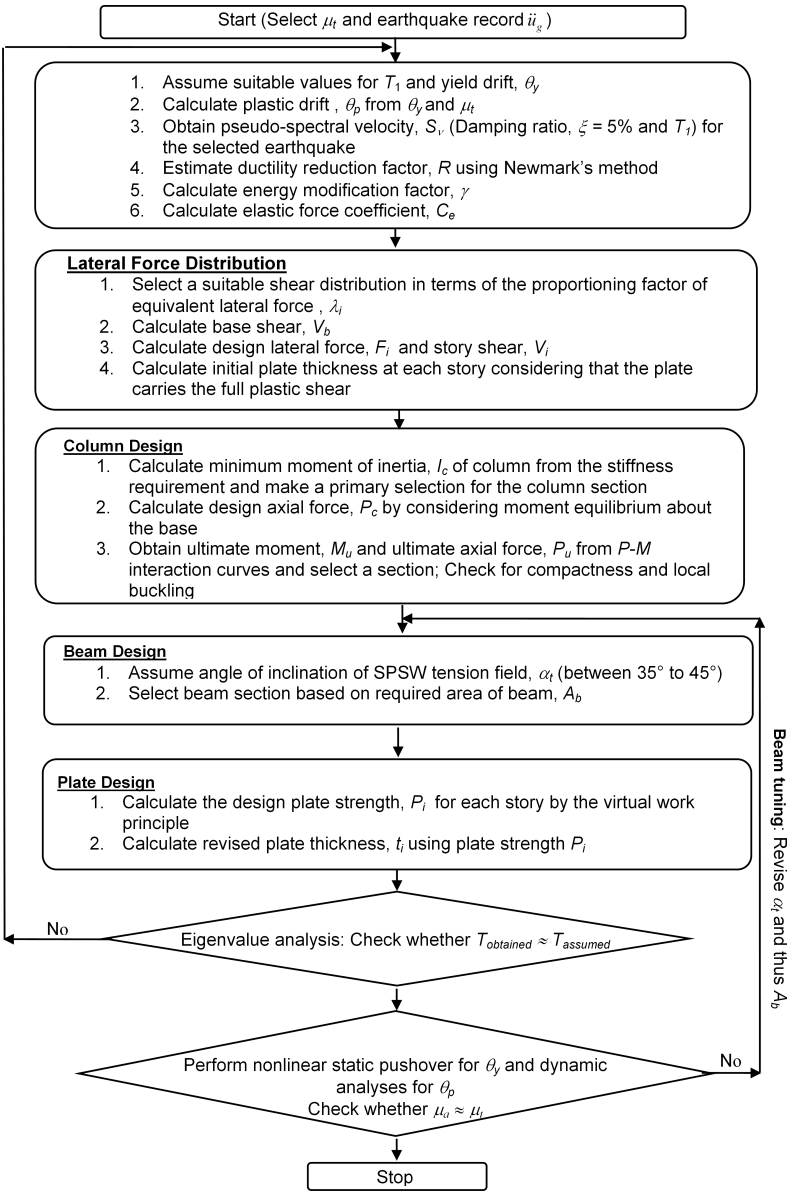

Fig. 4. Step-wise displacement-based design procedure for SPSW with rigid HBE–VBE connections.

(6) The preliminary thicknesses (t_i') of steel plates are calculated as:

$$t_i' = \frac{2V_i}{0.95F_yL}, \tag{9}$$

where V_i is the ith story shear, F_y is the yield stress of the plate material, and L is the width of the steel plate.

(7) Calculate the plastic design moment (M_{pc}) and axial force (P_c) in columns (VBE). Select the final column sections considering suitable P–M interaction, compactness, and local buckling requirements. Assume approximate beam (HBE) sections.
(8) Calculate required shear strength of plate (P_i) at each story by equating the internal and the external inelastic work. Obtain final thickness of plates (t_i):

$$t_i = \frac{2P_i}{0.95F_yL}. \tag{10}$$

(9) Perform an NLRHA of the structure subjected to the selected earthquake record and calculate μ_a. Tune the beam sections to bring μ_a closer to μ_t.

The design yield base shear is calculated by equating the external inelastic work done by the equivalent lateral forces with the internal plastic work done at the plastic hinges and through the plastification of the steel plate panels. For this, a specific lateral load distribution representing the distribution of equivalent static seismic forces at the plastic/mechanism state needs to be assumed. In the present work, several distributions are tried for each design scenario. These trial distributions represent code-specified time-invariant distributions that focus primarily on an elastic force-based design, and also recommendations for PBPD, where the inelastic behavior is incorporated in the design procedure. Among the code-specified distributions, the following three are selected which can be described by Eq. (2):

(1) "UBC," following the UBC [ICBO, 1997], with $k = 1$.
(2) "IS," following the Indian Standard [BIS, 2002], with $k = 2$.
(3) "IBC," following the IBC [ICC, 2006], where k is a function of T_1.

Among the PBPD distributions, two are selected which can be described by Eq. (3):

(1) "Lee," proposed by Lee and Goel [2001], with $\alpha = 0.5$.
(2) "Chao," proposed by Chao *et al.* [2007], with $\alpha = 0.75$.

A wide variety of design scenarios is selected for checking the effectiveness of these five trial distributions. The design scenarios include three building configurations:

(1) A four-story SPSW with pin-connected HBEs (or beams).
(2) A six-story SPSW with pin-connected HBEs.
(3) A four-story SPSW with rigid-connected HBEs (to the VBEs or columns).

The six-story SPSW is included in the case study so as to see if a vibration mode, other than the fundamental one, has any significant effect on the effectiveness of a lateral force distribution used for the PBPD. The four-story SPSW with rigid HBE–VBE connections has a fundamental difference in configuration and plastic hinging from those of the four-story SPSW with pin-connected HBEs. Moreover, the design method changes slightly for an SPSW with rigid HBE–VBE connections from an SPSW with pinned beams. The scenarios also include two to three different

Table 1. Details of earthquake records used for design.

Earthquake	Date	Station	Component	PGA(g)	Code used
Northridge	Jan. 17, 1994	Sylmar Converter	Horizontal-052	0.612	SYL
Kobe	Jan. 16, 1995	KJMA	Horizontal-000	0.812	KJM
Kobe	Jan. 16, 1995	Takarazuka	Horizontal-000	0.692	TAZ

plate panel aspect ratios (story height to bay length $= h_s/L$) for each of the building configurations mentioned above. Two to three strong ground motions are considered for these designs and the subsequent checking of theirs. Details of the records are provided in Table 1 and Fig. 5 shows their ground acceleration time-history. The design scenarios also include different target ductility ratios (μ_t) ranging from 2.0 to 5.0. Altogether, 38 individual designs are considered, each of which are tried with the five distributions mentioned earlier. These generate a sufficiently large statistics on which the conclusions of this study are based.

2.1. *Design and analysis details*

Plan and elevations of the three selected buildings are shown in Fig. 6, which also shows the location of the SPSW and connection types between the HBE and VBE, and for the gravity frames (these frames are shown as dashed lines). The length of the SPSW bay is varied in order to achieve different aspect ratios (h_s/L = 1:1, 1:1.5, and 1:2), while keeping the other bay lengths constant. The designs are achieved by the steps shown in Figs. 3 and 4 [Ghosh *et al.*, 2009; Kharmale and Ghosh, 2010]. The lateral force vector $\mathbf{f}$ is obtained from the selected trial distribution and thus five alternate designs are achieved for each design scenario. Table 2 shows calculated values of design parameters at every step of a sample design scenario; for:

- The four-story SPSW with pin-connected HBEs.
- Aspect ratio = 1:1.
- Earthquake record: SYL.
- Target ductility ratio, $\mu_t = 3$.

This table gives the final required capacities of the members (SPSW, HBE, and VBE) for five alternative distributions of $\mathbf{f}$. A 5% Rayleigh damping is used in the design process, considering the design's focus on the plastic state of a structure.

As mentioned earlier, an NSPA and an NLRHA are conducted to calculate the achieved ductility ratio (μ_a). Both the analyses are performed using the structural analysis program DRAIN-2DX [Prakash *et al.*, 1993]. A multi-strip modeling scheme [Thorburn *et al.*, 1983] is used for the SPSW, where the plate is idealized with nonlinear truss elements and the boundary elements are modeled with nonlinear beam–column elements. At least 10 strips/truss elements are used to model every steel plate panel. A significant departure from the analyses performed by Ghosh *et al.* [2009] is that the actual inclination angles for these strips (α_t) are used instead of their mean over all the stories [Gupta *et al.*, 2009]. The rigid floor

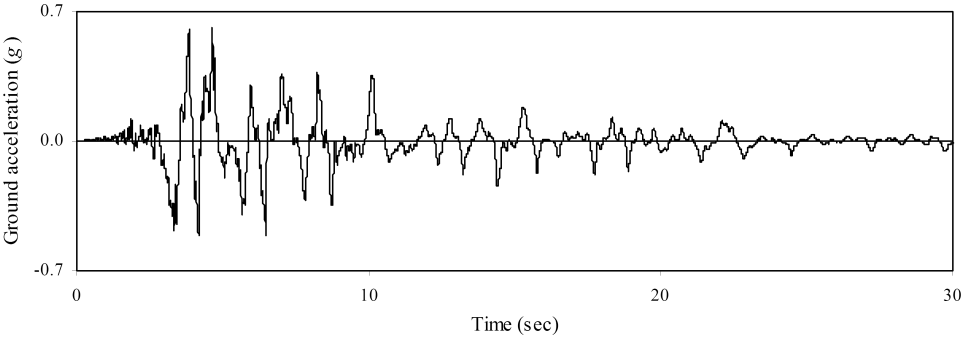

(a)

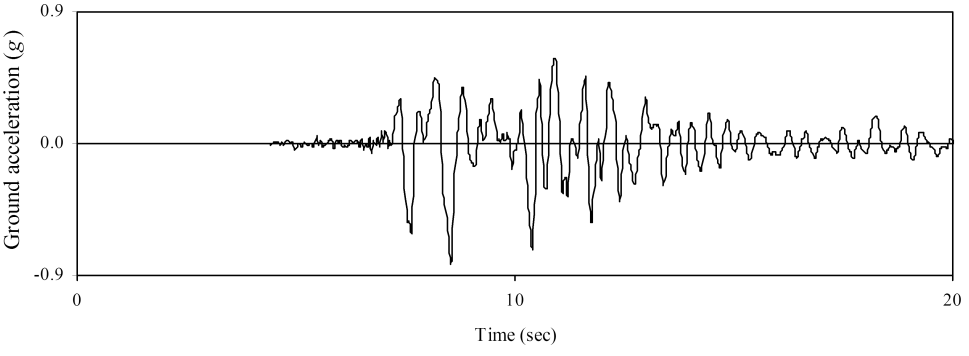

(b)

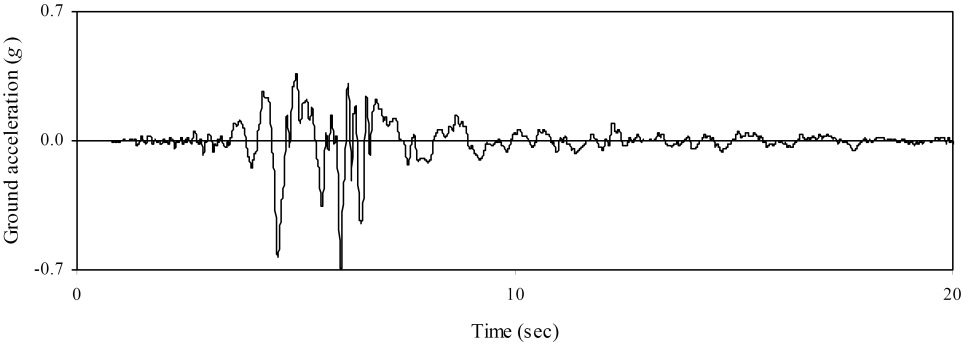

(c)

Fig. 5. Ground acceleration time-histories for (a) SYL, (b) KJM, and (c) TAZ.

diaphragm effect is considered at all the floor levels. The material used is elastic-perfectly plastic steel with a yield strength of 344.74 MPa (=50 ksi) and without any overstrength factor. No geometric nonlinearity is considered in the analysis procedure. Effect of gravity loads, lateral stiffness of gravity frame members, and flexibility of the joint panel zones are neglected in the analyses. For the NLRHA, a

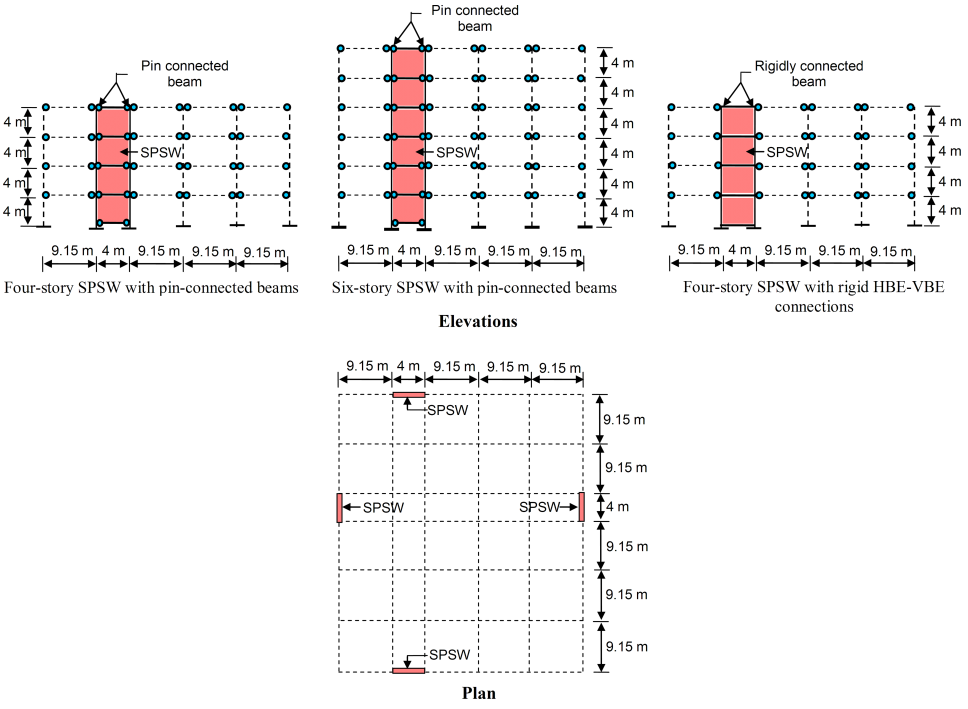

Fig. 6. Plan and elevations of the three study buildings showing the SPSW locations and connections.

lumped mass model is considered. 5% Rayleigh damping is assigned to the first two modes. Strength and stiffness degradations are neglected in the hysteresis behavior.

3. Results and Comparison

The alternative designs for each design scenario are compared primarily in terms of the closeness of the achieved ductility ratio (μ_a) to the target ductility ratio (μ_t). The difference between the two is measured as a percentage:

$$\% \text{ Diff.} = \frac{\mu_a - \mu_t}{\mu_t} \times 100. \tag{11}$$

Tables 3 to 9 give the results in detail in terms of this difference for each alternative in a design scenario. A parameter "AbsMax" is defined that gives the absolute maximum error (% Diff.) among all the design scenarios for a typical building configuration. For a typical design scenario, the % Diff. is compared among several trial distributions and for a selected building configuration the AbsMax and the average of % Diff. values are compared among these distributions. This average is primarily used as a measure of the effectiveness of a force distribution formula. For the four-story building with pin-connected HBEs and a plate aspect ratio 1:1 (Table 3), the

Table 2. Design calculations for a sample design (Design II).

Common design parameters					
Aspect ratio, h_s/L					1:1
Selected earthquake record					SYL
Target ductility ratio, μ_t					3.0
Assumed yield drift, θ_y(rad)					1%
Plastic drift, θ_p(rad)					2%
Fundamental time period, T_1(s)					0.75
Pseudo velocity, S_v, corresponding to T_1 and $\xi = 5\%$ (m/s)					2.07
Normalized design pseudo acceleration, S_a/g (m/s^2)					1.76
Ductility reduction factor, R_μ					3.0
Energy modification factor, γ					0.56
Total seismic weight, W (kN)					19,170
Design calculations for selected shear distributions					
	UBC	IBC	IS	Lee	Chao
Base shear (kN), V_b	8,471	8,360	7,791	7,695	8,142
Equivalent lateral force (kN), f_4	3,554	3,660	4,311	4,858	4,084
f_3	2,548	2,442	2,237	1,560	2,117
f_2	1,639	1,548	994	874	1,309
f_1	819	710	249	404	632
Story shear (kN), V_4	3,554	3,660	4,311	4,858	4,084
V_3	6,012	6,103	6,548	6,417	6,201
V_2	7,651	7,650	7,542	7,291	7,510
V_1	8,471	8,360	7,791	7,695	8,142
Plate thickness (mm), t_4	4.98	5.14	6.09	6.85	5.75
t_3	8.43	8.56	9.26	9.05	8.70
t_2	10.7	10.7	10.7	10.3	10.6
t_1	11.9	11.7	11.0	10.8	11.5
VBE moment (10^4 kNm), M_{pc}	2.36	2.37	2.42	2.42	2.39
VBE axial force (10^3 kN), P	4.23	4.18	3.89	4.05	4.07
VBE ultimate moment (10^4 kNm), M_u	3.33	3.33	3.32	3.35	3.32
VBE ultimate axial force (10^4 kN), P_u	1.23	1.23	1.23	1.24	1.23
VBE section	W 36 × 529	W 36 × 529	W 36 × 529	W 36 × 529	W 40 × 503
HBE section	W 12 × 152	W 14 × 145	W 12 × 136	W 14 × 90	W 14 × 145

average value of percentage difference varies within a narrow range from −4.13 to −1.68 for all the five distributions. Even the absolute maximum percentage difference (AbsMax) varies in a short range of 16.3–20.0. These results signify that for these six designs (Designs I–VI), with different target ductility values and considering different acceleration records, the five different trial distributions yield similar results in terms of the ductility calculated on the basis of the roof displacement. Table 4 presents this comparison for the same four-story pin-connected structure, but with a different steel panel aspect ratio (h_s/L = 1:1.5). For these six designs (Designs VII–XII), the average percentage difference is found to vary, again, within a narrow range of −6.84 to −2.31. For Designs XIII–XVII (Table 5), for the same

Table 3. Results summary for designs of four-story SPSW with pin-connected beams for $h_s/L = 1:1$.

			UBC		IBC		IS		Lee		Chao	
Design	Record	μ_t	μ_a	% Diff.	μ_a	% Diff.	μ_a	% Diff.	μ_a	% Diff.	μ_a	% Diff.
I	SYL	2	2.09	4.50	2.04	2.00	1.99	−0.500	2.11	5.50	2.01	0.500
II	SYL	3	3.05	1.67	3.00	0.00	2.93	−2.33	3.04	1.33	3.01	0.333
III	SYL	4	3.99	−0.250	3.77	−5.75	3.79	−5.25	3.64	−9.00	3.58	−10.5
IV	KJM	2	1.98	−1.00	2.07	3.50	2.04	2.00	1.95	−2.50	2.02	1.00
V	KJM	3	3.04	1.33	3.04	1.33	3.07	2.33	2.99	−0.333	3.06	2.00
VI	KJM	4	3.35	−16.3	3.30	−17.5	3.20	−20.0	3.21	−19.8	3.32	−17.0
Average				−1.68		−2.74		−3.96		−4.13		−3.95
AbsMax				16.3		17.5		20.0		19.8		17.0

Table 4. Results summary for designs of four-story SPSW with pin-connected beams for $h_s/L = 1:1.5$.

			UBC		IBC		IS		Lee		Chao	
Design	Record	μ_t	μ_a	% Diff.	μ_a	% Diff.	μ_a	% Diff.	μ_a	% Diff.	μ_a	% Diff.
VII	SYL	2	2.08	4.00	1.98	−1.00	2.03	1.50	1.90	−5.00	2.05	2.50
VII	SYL	3	3.03	1.00	3.01	0.333	2.97	−1.00	3.23	7.67	2.94	−2.00
IX	SYL	4	3.94	−1.50	3.96	−1.00	4.05	1.25	3.80	−5.00	4.00	0.000
X	KJM	2	1.98	−1.00	1.98	−1.00	2.04	2.00	1.96	−2.00	2.02	1.00
XI	KJM	3	2.99	−0.333	2.96	−1.33	2.76	−8.00	2.68	−10.7	2.87	−4.33
XII	KJM	4	3.36	−16.0	3.43	−14.3	3.51	−12.3	3.01	−24.8	3.43	−14.3
Average				−2.31		−3.05		−2.76		−6.64		−2.86
AbsMax				16.0		14.3		12.3		24.8		14.3

Table 5. Results summary for designs of four-story SPSW with pin-connected beams for $h_s/L = 1:2$.

			UBC		IBC		IS		Lee		Chao	
Design	Record	μ_t	μ_a	% Diff.	μ_a	% Diff.	μ_a	% Diff.	μ_a	% Diff.	μ_a	% Diff.
XIII	SYL	2	2.01	0.500	2.05	2.50	2.01	0.500	1.92	−4.00	2.03	1.50
XIV	SYL	3	3.05	1.67	3.03	1.00	3.03	0.667	3.11	3.67	3.03	1.00
XV	SYL	4	3.67	−8.25	3.60	−10.0	3.62	−9.50	3.75	−6.25	3.56	−11.0
XVI	KJM	2	2.04	2.00	2.00	0.00	2.02	1.00	2.17	8.50	2.03	1.50
XVII	KJM	3	3.40	13.3	3.39	13.0	3.17	5.67	3.15	5.00	3.21	7.00
XVIII	KJM	4	3.57	−10.8	3.53	−11.8	3.60	−10.0	3.60	−10.0	3.43	−14.3
Average				−0.263		−0.883		−1.94		−0.513		−2.38
AbsMax				13.3		13.0		10.0		10.0		14.3

four-story structure but with a steel panel aspect ratio 1:2, this variation is within even a narrower range of −2.38 to −0.263. The AbsMax values for these five distributions also do not vary significantly enough. These three tables clearly show that for the four-story SPSW system with pin-connected HBEs, all the trial distributions are almost equally effective in achieving the target ductility ratio.

The other measure of the effectiveness of a distribution in these plastic designs, in addition to the roof displacement ductility, is the closeness of the yield/failure

Table 6. Results summary for designs of six-story SPSW with pin-connected beams for $h_s/L = 1:1$.

			UBC		IBC		IS		Lee		Chao	
Design	Record	μ_t	μ_a	% Diff.	μ_a	% Diff.	μ_a	% Diff.	μ_a	% Diff.	μ_a	% Diff.
XIX	SYL	3	3.02	0.667	3.12	4.00	3.13	4.33	3.09	3.00	3.07	2.33
XX	SYL	4	3.91	−2.25	3.96	−1.00	3.88	−3.00	4.00	0.000	4.05	1.25
XXI	SYL	5	5.01	0.200	5.03	0.600	4.99	−0.200	5.02	0.400	5.00	0.000
XXII	TAZ	3	3.02	0.667	2.95	−1.67	2.89	−3.67	2.97	−1.00	2.97	−1.00
XXIII	TAZ	4	3.42	−14.5	3.47	−13.3	3.48	−13.0	3.58	−10.5	3.58	−10.5
XXIV	TAZ	5	4.52	−9.60	4.51	−9.80	4.52	−9.60	4.49	−10.2	4.62	−7.60
Average				−4.14		−3.53		−4.19		−3.05		−2.59
AbsMax				14.5		13.3		13.0		10.5		10.5

Table 7. Results summary for designs of six-story SPSW with pin-connected beams for $h_s/L = 1:2$.

			UBC		IBC		IS		Lee		Chao	
Design	Record	μ_t	μ_a	% Diff.	μ_a	% Diff.	μ_a	% Diff.	μ_a	% Diff.	μ_a	% Diff.
XXV	SYL	3	2.97	−1.00	3.13	4.33	2.83	−5.67	3.03	1.00	3.17	5.67
XXVI	SYL	4	3.47	−13.3	3.64	−9.00	3.78	−5.50	3.49	−12.8	3.78	−5.50
XXVII	SYL	5	4.76	−4.80	4.73	−5.40	4.26	−14.8	4.40	−12.0	4.43	−11.4
XXVIII	TAZ	3	2.63	−12.3	2.58	−14.0	2.49	−17.0	2.57	−14.3	2.63	−12.3
XXIX	TAZ	4	3.81	−4.75	3.70	−7.50	3.56	−11.0	3.72	−7.00	3.64	−9.00
XXX	TAZ	5	4.65	−7.00	4.51	−9.80	4.43	−11.4	4.30	−14.0	4.42	−11.6
Average				−7.19		−6.90		−10.9		−9.85		−7.36
AbsMax				12.3		14.0		17.0		14.3		12.3

Table 8. Results summary for designs of four-story SPSW with rigid HBE–VBE connections for $h_s/L = 1:1$.

			UBC		IBC		IS		Lee		Chao	
Design	Record	μ_t	μ_a	% Diff.	μ_a	% Diff.	μ_a	% Diff.	μ_a	% Diff.	μ_a	% Diff.
XXXI	SYL	3	2.95	−1.67	3.24	8.00	3.06	2.00	3.12	4.00	3.17	5.67
XXXII	SYL	4	4.04	1.00	3.89	−2.75	3.92	−2.00	3.94	−1.50	3.94	−1.50
XXXIII	KJM	3	2.99	−0.333	3.03	1.00	2.89	−3.67	3.03	1.00	3.13	4.33
XXXIV	KJM	4	3.45	−13.8	3.56	−11.0	3.76	−6.00	3.72	−7.00	3.45	−13.8
Average				−3.69		−1.19		−2.42		−0.889		−1.31
AbsMax				13.8		11.0		6.00		7.00		13.8

mechanism formed (as per the NLRHA subjected to the design acceleration record) to the selected yield mechanism. Recollecting from Sec. 2, the target yield mechanism for this work implies a uniform interstory drift distribution over the height of the structure, which in turn implies a linear (i.e., inverted triangular) deformation shape. Therefore, for each design scenario, the deformed shape of the structure is obtained at the peak (roof displacement) response during the NLRHA and its closeness to a straight line is checked. This closeness is compared among the five selected trial distributions, graphically. Figure 7, for example, presents this comparison for the design scenarios Design II and XVIII. The deformation shapes are

Table 9. Results summary for designs of four-story SPSW with rigid HBE–VBE connections for $h_s/L = 1:2$.

			UBC		IBC		IS		Lee		Chao	
Design	Record	μ_t	μ_a	% Diff.	μ_a	% Diff.	μ_a	% Diff.	μ_a	% Diff.	μ_a	% Diff.
XXXV	SYL	3	3.07	2.33	2.92	−2.67	3.04	1.33	3.03	1.00	2.96	−1.00
XXXVI	SYL	4	3.72	−7.00	3.76	−6.00	3.87	−3.25	3.99	−0.250	3.84	−4.00
XXXVII	KJM	3	2.97	−1.00	2.95	−1.67	2.79	−7.00	2.87	−4.33	2.84	−5.33
XXXVIII	KJM	4	3.94	−1.50	3.93	−1.75	3.84	−4.00	3.82	−4.50	3.75	−6.25
Average				−1.79		−3.02		−3.23		−2.02		−4.23
AbsMax				7.00		6.00		7.00		4.50		6.30

obtained from an NLRHA using the acceleration record the structure is designed for (i.e., SYL and KJM, respectively). These plots show that the failure mechanisms obtained from different trial distributions are necessarily the same with minor differences in the amount of plastic rotations in individual stories. The deformation shapes are also close to an ideal straight line.

The closeness to the target is checked, in terms of the roof displacement ductility and failure mechanism, for design scenarios belonging to the other two study structures as well. For the six-story SPSW structure with pin-connected HBEs, two panel aspect ratios (1:1 and 1:2), two ground motion records (SYL and TAZ), and three values of μ_t (3.0, 4.0, and 5.0) are considered. For the structure with $h_s/L =$ 1:1, the average % Diff. varies in a narrow range of −4.59 to −2.19 (Table 6) and for the structure with $h_s/L = 1:2$, this range is also not a wide one: −10.9 to −6.90 (Table 7). Similar to the average values, the AbsMax also varies within a narrow range for all the five selected trial distributions. In addition to these two parameters, the deformation shapes are also compared among the selected trial distributions to check for any local (story-level) concentration of plasticity. Figure 8 shows sample maximum deformation plots for two design scenarios (Design XIX and XXII). It should be noted that even for this six-story SPSW, where the contribution of the fundamental mode to the (elastic) response of the system is expected to reduce (in a relative sense), the interstory drift distributions are close to uniform, implying a yield mechanism as per the design assumptions.

Similar results are also observed for the four-storied SPSW structure with rigid HBE–VBE connections. The primary reason to test this structure is to check the effectiveness of each selected trial distribution, considering the changes in the design procedure. For the designs with $h_s/L = 1:1$, the average % Diff. varies between −3.69 and −0.889 (Table 8), and for designs with $h_s/L = 1:2$ this average varies from −4.23 to −1.79 (Table 9). The AbsMax values are also presented in these two tables. The difference in these results among the five selected trial distributions are insignificant from a designer's perspective. Sample maximum deformation plots for the four-story structure with rigid VBE–HBE connections are presented in Fig. 9. These plots show, similar to the maximum deformation plots for the other two structures, that all the trial distributions give close-to-uniform drift distributions

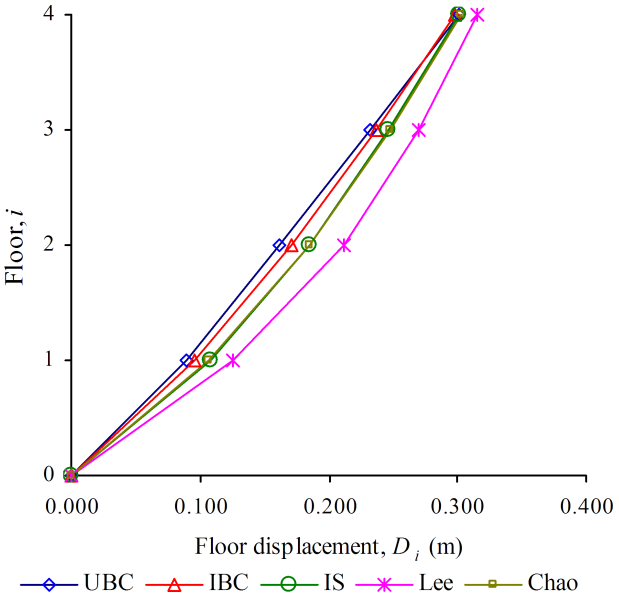

(a)

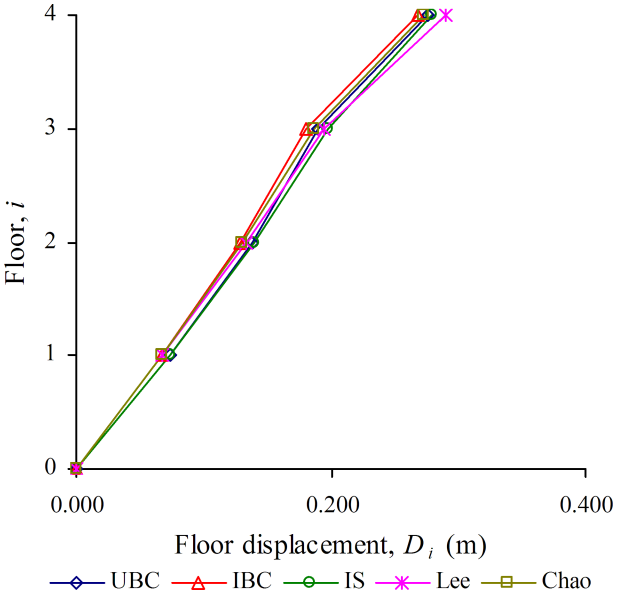

(b)

Fig. 7. Deformed shapes obtained for selected trial distributions for: (a) Design II and (b) Design XVIII of the four-story SPSW with pin-connected HBEs.

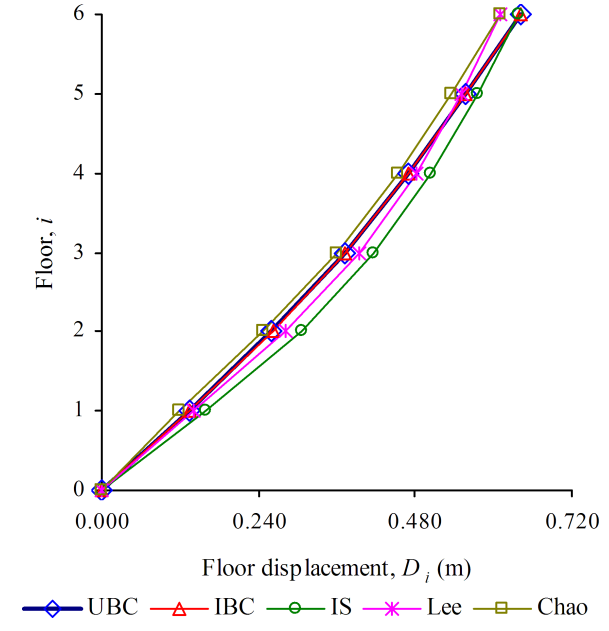

(a)

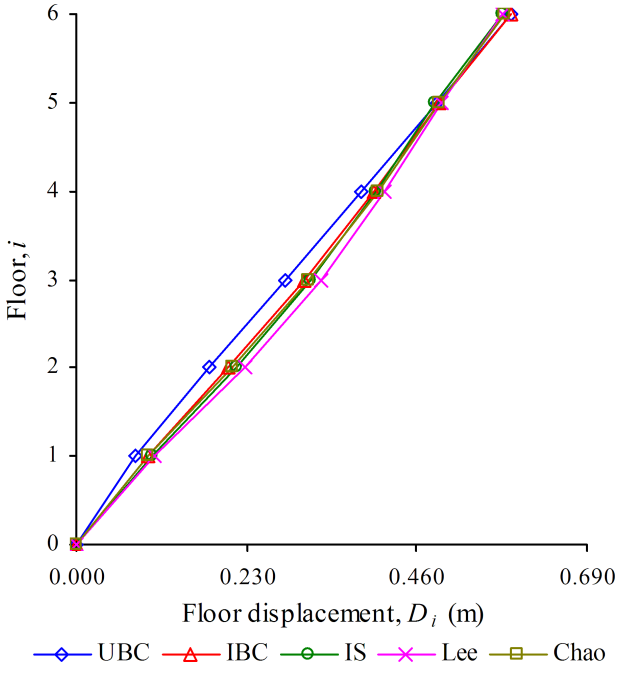

(b)

Fig. 8. Deformed shapes obtained for selected trial distributions for: (a) Design XIX and (b) Design XXII of the six-story SPSW with pin-connected HBEs.

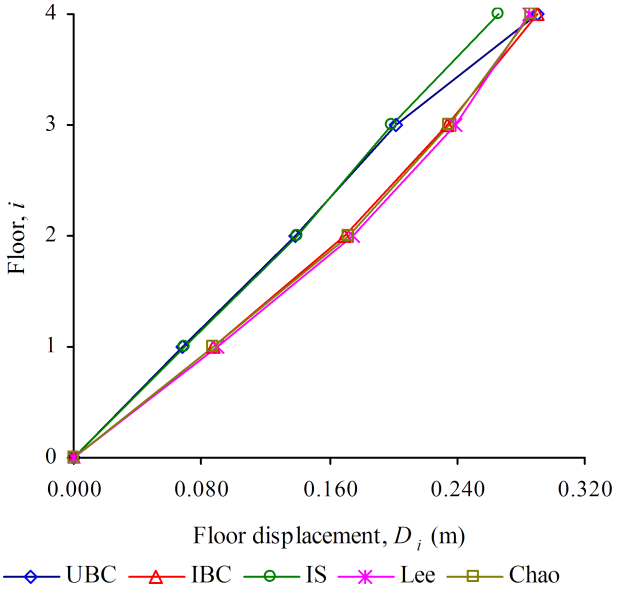

(a)

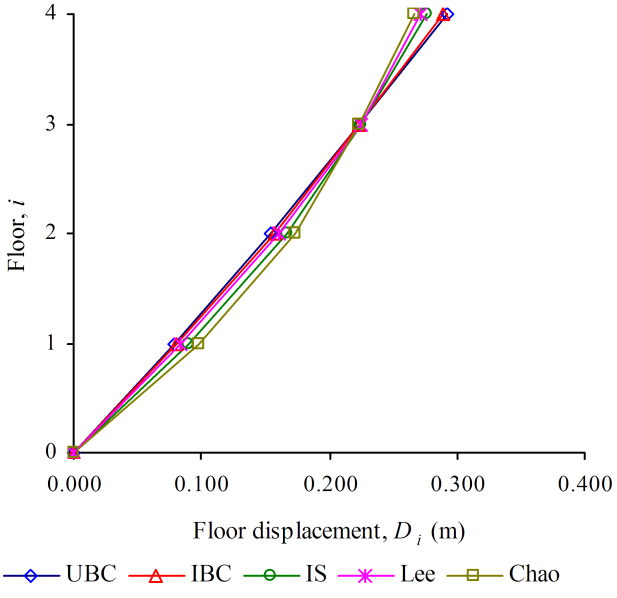

(b)

Fig. 9. Deformed shapes obtained for selected trial distributions for: (a) Design XXXIII and (b) Design XXXVIII of the four-story SPSW with rigid HBE–VBE connections.

over the height of the structure and achieve the target roof displacement ductility to a similar level of closeness.

4. Discussion on the Results

The results presented in the previous section very distinctly show that in terms of achieving the target ductility ratio, all the five trial distributions are equally effective. This is found to be true for low- to mid-rise structures and for different SPSW configurations. The primary argument in favor of this behavior is that when a structure reaches mechanism, its behavior (at least the deformation shape) is governed more by its inelastic capacities than its elastic mode shapes. To elaborate, the plastic shear capacities at each story of the structure, and not its fundamental or any other elastic mode shape (or any combination thereof), determine the distribution of story shears at the state of mechanism. If a structure, during its dynamic shaking subjected to base acceleration, achieves mechanism, then plastic shear capacities should be reached at each story. However, a typical mechanism may not be exactly attained by the structure at the instant of maximum roof displacement, and the actual story shear distribution at this state is expected to be only close to the shear distribution assumed in the design process, and not exactly be the same. Story shear values assumed in the design process (or, the "Design" story shears) are compared with the story shears at the instant of maximum roof displacement ("Actual" story shears) from the NLRHA. Sample comparison plots for different design scenarios are provided in Figs. 10–12. In each plot, the "Design" and the "Actual" story shear distributions are shown, respectively, using dashed and continuous lines of the same type. The design story shears are based on the design requirements (similar to Table 2), and are not exactly the story shear capacities for the structure. One reason for this difference is that the design story shears do not include the shear resisted by the boundary columns (and also does not consider the actual sections selected). An NSPA is the most common method to obtain the story shear capacities, but the capacities obtained using this method depend on the lateral force distribution assumed in the NSPA. The plots in Figs. 10–12 show that the design and actual story shear distributions are not very different, which to some extent justifies the similarity in the effectiveness of various lateral load distributions.

For the interstory drift distributions plotted in Figs. 7–9, it is observed that the UBC distribution, more than any other distribution, achieves closely a uniform drift distribution over the height of a structure. Since the selected yield mechanism for all the designs considered is based on a linear deformation shape, which is also the basis of the UBC lateral force distribution, the UBC distribution is found to be the most effective in obtaining a uniform drift distribution. It should, however, be noted that in terms of the achieved ductility ratio, all the distributions are found to be equally effective.

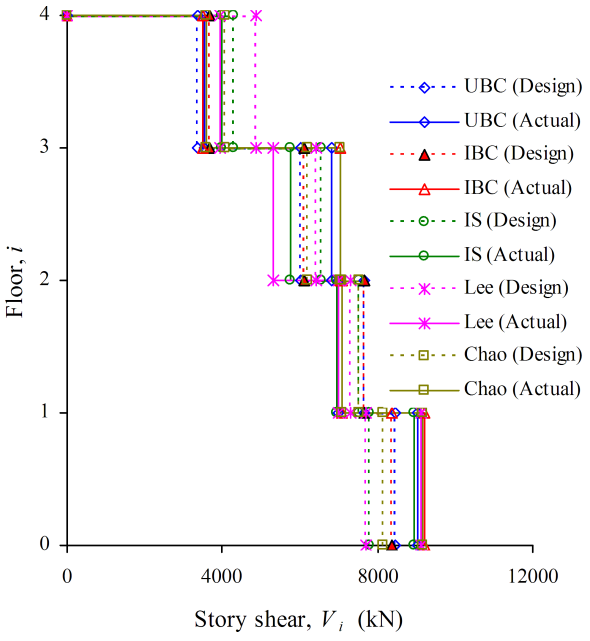

(a)

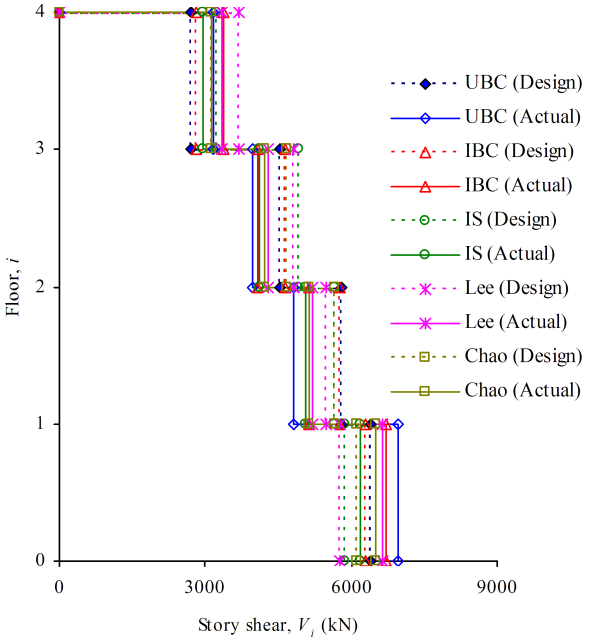

(b)

Fig. 10. Distributions of the "Design" and the "Actual" story shears for selected trial distributions for: (a) Design II and (b) Design XVIII of the four-story SPSW with pin-connected HBEs.

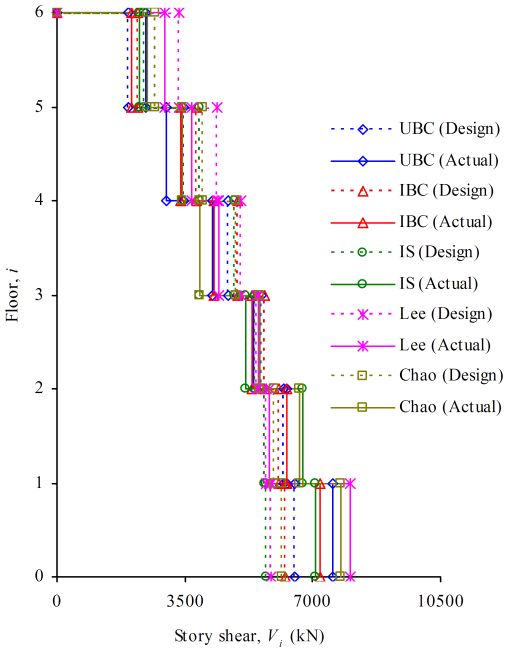

(a)

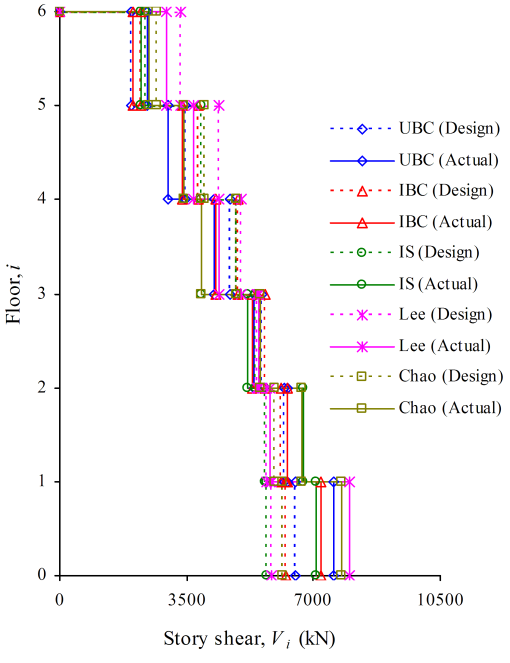

(b)

Fig. 11. Distributions of the "Design" and the "Actual" story shears for selected trial distributions for: (a) Design XIX and (b) Design XXII of the six-story SPSW with pin-connected HBEs.

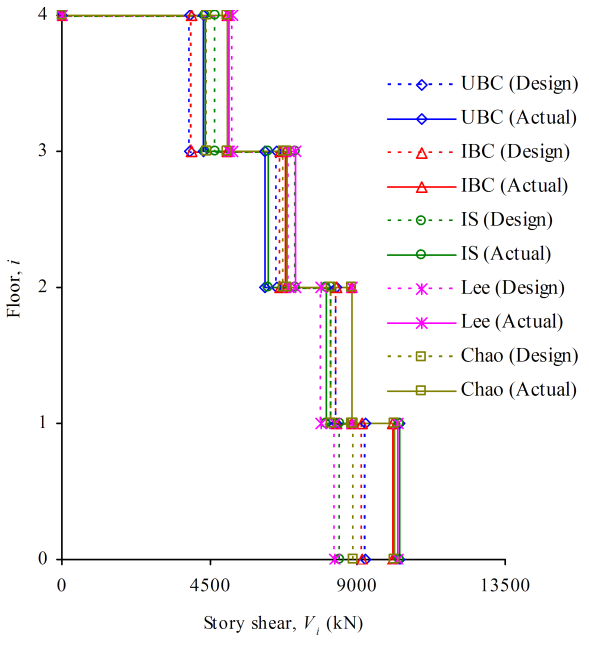

(a)

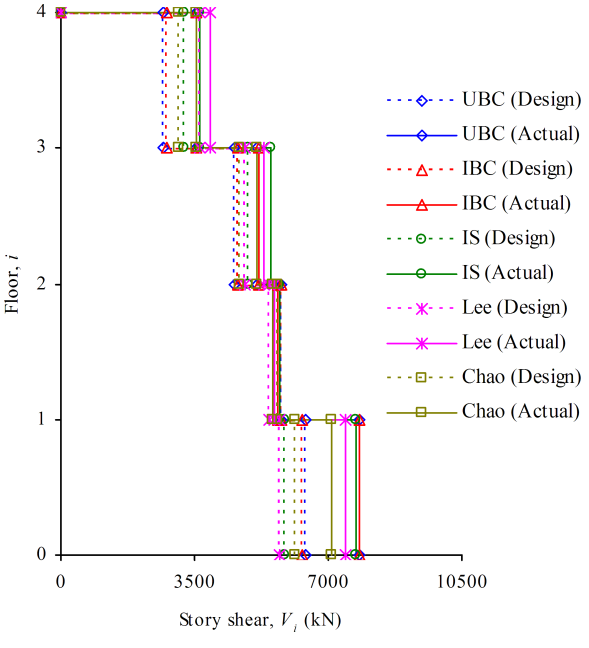

(b)

Fig. 12. Distributions of the "Design" and the "Actual" story shears for selected trial distributions for: (a) Design XXXIII and (b) Design XXXVIII of the four-story SPSW with rigid HBE–VBE connections.

5. Concluding Remarks

The search for a suitable lateral force distribution to be used in displacement-based plastic designs of SPSW systems is made using a trial-based approach. In this approach, five trial distributions are compared in terms of their effectiveness in meeting the plastic design targets. These trial designs are based on a large set of 38 design case studies — involving variations in SPSW configuration, building height, steel panel aspect ratio, design ground acceleration, and target ductility ratio. The effectiveness of a trial distribution is measured in terms of the closeness of the achieved ductility ratio to the target (based on the roof displacement) and the distribution of interstory drift over the height. Based on this large statistics of results, all the selected trial distributions are found to be almost equally effective. Therefore, it is recommended that any of the commonly adopted shear distributions (which are represented by the selected five) can be used for the plastic design of SPSW systems following Ghosh *et al.* [2009] and Kharmale and Ghosh [2010]. It should be noted that although a large variety of design scenarios are considered in the trial-based approach, this conclusion may not hold good for high-rise buildings. However, if the structure is designed for a large target ductility and it follows the plastic mechanism assumed in the design process closely, then any of the commonly adopted lateral force/story shear distributions can be adopted for the plastic design of these systems. It should also be noted here that the "UBC" distribution is found to be better, although not by a great margin, than any other distribution for achieving a uniform interstory drift over the height of the structure, and hence is recommended for that purpose. These conclusions should not be limited to the plastic design of SPSW systems only, but it needs to be validated through similar means (trial design for a sufficient variety of design scenarios) before applying to the plastic design of other building configurations.

Acknowledgment

Support for this research on developing displacement-based design methods for steel plate shear wall structures is provided by the Department of Science and Technology (DST), India. The findings and the opinions expressed herein are those of the authors and do not necessarily represent the views of DST.

References

ASCE [2005] *SEI/ASCE 7-05, Minimum Design Loads for Buildings and Other Structures (Including Supplement No. 1)* (American Society of Civil Engineers, Reston, USA).

BIS [2002] *IS 1893 (Part 1). Criteria for Earthquake Resistant Design of Structures, Part 1: General Provisions and Buildings* (Bureau of Indian Standards, New Delhi, India).

Chao, S.-H. and Goel, S. C. [2005] "Performance-based design of EBF using target drift and yield mechanism," *Research Report UMCEE 05-05* (University of Michigan, Ann Arbor, USA).

Chao, S.-H., Goel, S. C. and Lee, S.-S. [2007] "A seismic design lateral force distribution based on inelastic state of structures," *Earthquake Spectra* **23**(3), 547–569.

Chopra, A. K. and Goel, R. K. [2001] "Direct displacement-based design: Use of inelastic vs. elastic design spectra," *Earthquake Spectra* **17**(1), 47–64.

FEMA [2006] *Action Plan for Performance-Based Seismic Design* (*FEMA 445*) (Federal Emergency Management Agency, Washington, USA).

Ghosh, S., Das, A. and Adam, F. [2009] "Design of steel plate shear walls considering inelastic drift demand," *J. Constr. Steel Res.* **65**(7), 1431–1437.

Goel, S. C. and Chao, S.-H. [2009] *Performance-Based Plastic Design*: *Earthquake-Resistant Steel Structures* (International Code Council, Washington, USA).

Gupta, B. and Kunnath, S. K. [2000] "Adaptive spectra-based pushover procedure for seismic evaluation of structures," *Earthquake Spectra* **16**(2), 367–391.

Gupta, M. K., Kharmale, S. and Ghosh, S. [2009] "Ductility-based seismic design of steel plate shear walls: Practical application using standard sections," *Int. J. Adv. Struct. Eng.* **1**(2), 93–110.

ICBO [1997] *Uniform Building Code* (*UBC*) (International Conference of Building Officials, Whittier, USA).

ICC [2006] *International Building Code* (*IBC*) (International Code Council, Whittier, USA).

Kalkan, E. and Kunnath, S. [2006] "Adaptive modal combination procedure for nonlinear static analysis of building structures," *ASCE J. Struct. Eng.* **132**(11), 1721–1732.

Kalkan, E. and Kunnath, S. [2007] "Assessment of current nonlinear static procedures for seismic evaluation of buildings," *Eng. Struct.* **29**(3), 305–316.

Kharmale, S. B. and Ghosh, S. [2010] "Displacement-based seismic design of steel plate shear wall systems with rigid-connected beams," *9th US National and 10th Canadian Conf. on Earthquake Engineering* (Toronto, Canada).

Lee, S.-S. and Goel, S. C. [2001] "Performance-based design of steel moment frames using target drift and yield mechanism," *Research Report UMCEE 01-07* (University of Michigan, Ann Arbor, USA).

Newmark, N. M. and Hall, W. J. [1982] *Earthquake Spectra and Design* (Earthquake Engineering Research Institute, Berkeley, USA).

Prakash, V., Powell, G. H. and Campbell, S. [1993] "DRAIN-2DX, base program description and user guide: version 1.10," *Report No. UCB/SEMM-93/17* (University of California, Berkeley, USA).

SEAOC [1995] *Vision 2000*: *Performance Based Seismic Engineering of Buildings* (Structural Engineers Association of California, Sacramento, USA).

Shakeri, K., Shayanfar, M. A. and Kabeyasawa, T. [2010] "A story shear-based adaptive pushover procedure for estimating seismic demands of buildings," *Eng. Struct.* **32**(1), 174–183.

Thorburn, L. J., Kulak, G. L. and Montgomery, C. J. [1983] "Analysis of steel plate shear walls," *Structural Engineering Report No. 107* (Department of Civil Engineering, University of Alberta, Edmonton, Canada).